Soil emissivity and reflectance spectra measurements

José A. Sobrino,[1,*] Cristian Mattar,[1] Pablo Pardo,[2] Juan C. Jiménez-Muñoz,[1]
Simon J. Hook,[3] Alice Baldridge,[3] and Rafael Ibañez[2]

[1]Global Change Unit, Image Processing Laboratory, University of Valencia, P.O. Box 22085, Valencia E-46071, Spain

[2]Material Science Institute, University of Valencia, P.O. Box 22085, Valencia E-46071, Spain

[3]Jet Propulsion Laboratory, California Institute of Technology, Pasadena, California 91109, USA

*Corresponding author: sobrino@uv.es

Received 15 April 2009; accepted 20 May 2009;
posted 4 June 2009 (Doc. ID 109843); published 23 June 2009

We present an analysis of the laboratory reflectance and emissivity spectra of 11 soil samples collected on different field campaigns carried out over a diverse suite of test sites in Europe, North Africa, and South America from 2002 to 2008. Hemispherical reflectance spectra were measured from 2.0 to 14 μm with a Fourier transform infrared spectrometer, and x-ray diffraction analysis (XRD) was used to determine the mineralogical phases of the soil samples. Emissivity spectra were obtained from the hemispherical reflectance measurements using Kirchhoff's law and compared with *in situ* radiance measurements obtained with a CIMEL Electronique CE312-2 thermal radiometer and converted to emissivity using the Advanced Spaceborne Thermal Emission and Reflection Radiometer (ASTER) temperature and emissivity separation algorithm. The CIMEL has five narrow bands at approximately the same positions as the ASTER. Results show a root mean square error typically below 0.015 between laboratory emissivity measurements and emissivity measurements derived from the field radiometer. © 2009 Optical Society of America

OCIS codes: 120.0120, 120.0280, 300.6300.

1. Introduction

Land surface emissivity (LSE) plays an important role in thermal remote sensing, since it is an essential factor for calculating accurate measurements of surface temperature by radiometry (a 1% error in emissivity produces an error in the recovered surface temperature of 6 K in the absence of any balancing effect from the atmosphere) [1]. In addition, LSE is a useful indicator of the specific properties of the surface and provides important angular information that can also influence the estimation of the land surface temperature [2,3].

One of the most common ways to calculate emissivity (ε) is to convert directional hemispherical reflectance measurements to emissivity via Kirchhoff's law, $\varepsilon = 1 - R$, where R is the hemispherical reflectance [4]. Note the emissivity can only be recovered accurately from hemispherical measurements rather than biconical or bidirectional reflectance measurements [5,6], where the directional nature of the radiation measured by biconical reflectance does not adequately account for radiation scattered in all directions [4]. The emissivity of a surface can be measured in either emission or reflectance. When measured in emission, the sample must be heated to enhance the emission itself and minimize the reflection term, so reflectance measurements are used commonly, as, for example, the Arizona State University spectral library [7,8] or the Advanced Spaceborne Thermal Emission and Reflection Radiometer (ASTER) spectral library v 2.0 (ASL) [9,10]. The spectral libraries mentioned above present a large number of spectra but do not capture the variation observed in many soils. The current paper presents additional soil sample spectra from multiple test sites which can be used to validate spaceborne emissivity measurements from sensors such as the ASTER.

0003-6935/09/193664-07$15.00/0
© 2009 Optical Society of America

Table 1. Sample Characteristics

Projects	Time Period	Supported	Text Code	Place	Latitude	Longitude	Descriptions	USDA Soil Taxonomy
Sentinel-2 and Fluorescence Experiment (SEN2FLEX)	2005	European Space Agency (ESA)	BS	Barrax, Spain	39°3′ N	2°6′ W	characteristic bare soil with high clay content and poorly developed.	*inceptisol*
CarboEurope, Flex and Sentinel-2 (CEFLES-2)	2007–2008	ESA	B	Bordeaux, France	44°24′19″ N	0°36′14.6″ W	agriculture soil with high organic matter content	*spodosol*
			LL	Les Landes, France	44°27′24″ N	0°11′51″ E	agriculture baresoil	*inceptisol*
Agricultural bio/geophysical retrieval from frequent repeat pass SAR and optical imaging (AGRISAR)	2006	ESA	AG	Görmin, Germany	53°59′51″ N	13°16′45″ W	characteristic bare soil for annual crop	*mollisol*
Exploitation of angular effects in land surface observations from satellites (EAGLE)	2004–2007	European Union (EU)	H	Noordwijk, Holland	52°14′35″ N	4°25′39″ E	red sand with high content of salts	*entisol*
HYDRA reconstructing historical dynamic of marsh flood in Doñana using remote sensing.	2008	Ministerio de Ciencia y Tecnología, España	D1	Doñana National Park, Spain	36°58′49″ N	6°29′48.3″ W	coastal sand	*entisol*
			D2		37°4′18″ N	6°16′54″ W	yellow sand used for bull ring	*entisol*
Visit to Pastoruri glacier[a]	2008	CONIDA	P	Pastoruri, Perú	9°54′32.2″ S	77°10′58″ W	bare soil near glaciers	*rock/lands near ice glaciers*
Mount Hudson Field Campaign[b]	2002	Chilean volcanos research field campaign	CH	Hudson, Chile	45°54′ S	72°58′ W	volcanic ash	*rock/lands near ice glaciers*
Dual-use European Security IR Experiment (DESIREX)	2008	ESA	MD	Madrid, Spain	40°32′52″ N	3°41′49″ W	soccer field bare soil	*inceptisol*
Water use efficiency in natural vegetation and agricultural areas by remote sensing in the Mediterranean basin (WATERMED)	1999–2002	EU	M 131	Marrakech, Morocco	31°40′ N	7°35′ W	agriculture bare soil with high clay content	*leptosols, regosols (LP)*

[a]P samples were collected during a visit to Pastoruri glacier in the framework of Comisión Nacional de Investigación y Desarrollo Aeroespacial (CONIDA) of Perú regional activities.

Table 2. Mineralogical Phases Of Soil Samples Analyzed With XRD[a]

	Quartz	Calcite	Feldspar	Dolomite	Sheet-Silicates
AG	*X*		•		
B	*X*		•		
BS	•	*X*			
CH	•		*X*	•	
D1	*X*				
D2	*X*	•			
H	*X*		•		
LL	*X*				•
M131	*X*	•	•		•
MD	*X*		•		
P	*X*				•

[a](*X*), main phases; (•), rest of identified minerals

The aim of this paper is to present soil emissivity spectra corresponding to several sites that have been used in field campaigns undertaken by the Global Change Unit (GCU) from the University of Valencia. These samples were subjected to mineralogical and spectral analysis as well as radiometric comparison with ground-based measurements carried out with thermal radiometers. Note that, in addition to the spectral characterization of soil samples, the emissivity spectra presented in this paper can be used for validation of temperature and emissivity separation algorithms that can be applied to a number of airborne and spaceborne sensors that have also been used to acquire data over the sites. This work is organized as follows: Section 2 includes the soil samples description, and describes the experimental setup and instruments used to retrieve reflectance/emissivity spectra and mineralogical characteristics, Section 3 shows the results obtained, and, finally, Section 4 summarizes the main conclusions drawn from this study.

2. Sample Description and Experimental Setup

The soil samples used in this study were acquired during several remote sensing field campaigns carried out between 2002 and 2008. Characteristics for the samples are provided in Table 1. This table also provides a brief text code for each sample, which will be used throughout the paper for simplification in the notation. The emissivity spectra of the soil samples were obtained from hemispherical reflectance measurements carried out at the Jet Propulsion Laboratory (JPL) in Pasadena, California, USA, and converted to emissivity using Kirchhoff's law [11]. Measurements were made of each soil sample using a Nicolet 520 Fourier transform infrared (FT-IR) spectrometer equipped with a Labsphere integrating sphere. One thousand scans at $4\,cm^{-1}$ spectral resolution were acquired over ~15 min/sample and averaged together. A background spectrum was acquired using a diffuse gold plate and used to remove background radiation from the sample spectrum. Other equipment characteristics and sample preparation protocols are detailed in Baldridge *et al.* [9].

To determine mineralogical soil composition, x-ray diffraction (XRD) analyses were carried out. For this purpose, soil samples were first oven dried at 40 °C during 24 h to eliminate humidity content. After that, a Fritsch Pulverisette 9 vibrating cup mill was used for dry grinding loads of ~10 g of the material using a 100 ml tungsten carbide coated stainless steel set of cup, ring, and cylinder. Milling time to prepare soil samples for XRD analysis was 3 s. X-ray powder diffraction scans were performed between 5° and 65° 2θ with a step size of 0.05° 2θ and a 5 s counting time in a copper-anode Bruker D5000 diffractometer, working at 40 kV and 30 mA, with a Ni filter, a 1° divergence slit, a 1° antiscattering slit, a graphite diffracted beam monochromator, and a scintillation detector. EVA software (part of Diffrac-Plus suite of Bruker AX Systems) was used for the mineralogical characterization.

3. Results

A. X-Ray Diffraction Analysis

The XRD analysis results are shown in Table 2, which presents the predominant crystalline phases of each sample. The most frequently found minerals were quartz (SiO_2), which usually occurs with feldspar, and calcite ($CaCO_3$). Sands like H or D1 contain a high proportion of crystalline quartz, which is manifest in the emissivity spectra. Sample CH contains a calicium-rich plagioclase feldspar anorthite ($CaAl_2Si_2O_8$), dolomite $CaMg(CO_3)_2$, and quartz. Finally, M131 has four crystalline phases, in addition to quartz and calcite, anorthite, and illite ($2K_2O\cdot 3MgO\cdot Al_2O_3\cdot 24SiO_2\cdot 12H_2O$). Samples P and LL correspond to sandstones with a significant clay content.

B. Reflectance and Emissivity Spectra from FT-IR Spectroscopy

Reflectance spectra between 2 and 14 μm and emissivity spectra between 8 and 14 μm for each soil sample are shown in Fig. 1. Sands (H, D1) and MD, with the presence of quartz, is indicated by a Christiansen peak near 12.3 μm, and another relative peak is evidenced at 7.4 μm. This peak occurs in a part of the electromagnetic spectrum where terrestrial measurements of atmospheric water vapor have very strong emission/absorption bands. Because of this limitation the feature has been used for mapping with planetary datasets whereas, with terrestrial datasets, the adjacent emissivity minimum that falls within a clear part of the electromagnetic spectrum [4,12] is used. The minimum values in the reststrahlen bands (8.0 and 9.0 μm), where the absorption coefficient is high, are clearly apparent in the spectra. Similar results were observed for a quartz sample in [5]. Other samples, such as AG and B, present quartz as the main phase but the Christiansen peak and minimum of reststrahlen are relatively diffuse in relation to H and D1. This is attributed to the presence of other minerals, in particular feldspar, which may have had an influence on the hemispherical

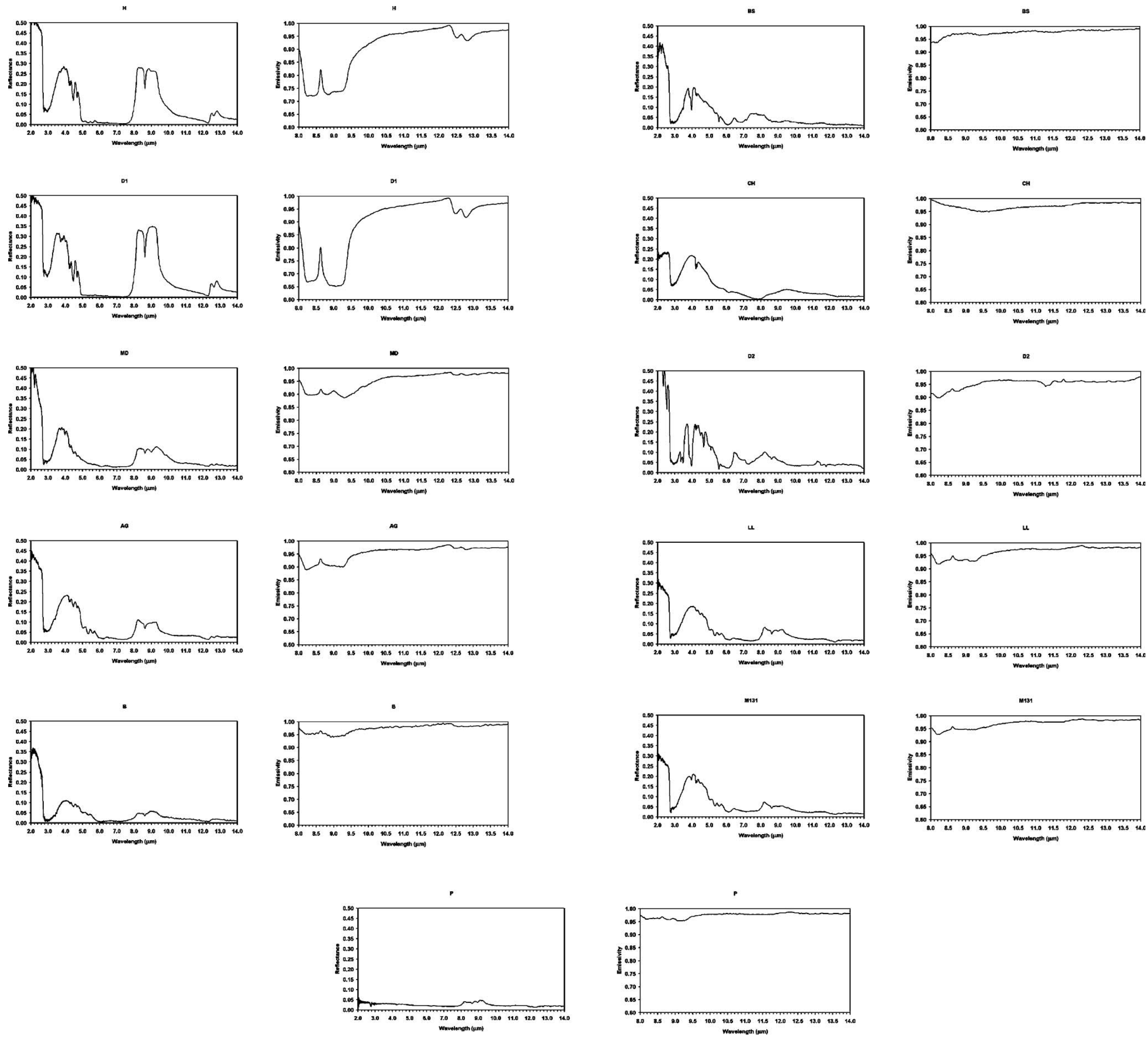

Fig. 1. Reflectance between 2.0 and 14.0 μm (left column) and emissivity between 8.0 and 14.0 μm (right column) for each soil.

reflectance in that region. The rest of the samples show several spectral features since they contain at least three mineralogical phases.

C. Comparison with Samples Included in the ASTER Spectral Library

The emissivity spectra presented in this paper have been compared to other soil emissivity spectra included in the ASL. Currently, the ASL has more than 69 soil spectra classified according to United States Department of Agriculture (USDA) taxonomy soil classes. Additionally, ancillary data, such as mineralogical and spectroscopy descriptions, are also provided for some samples.

The ASL spectra were convolved with the system response of the ASTER instrument to obtain band-averaged values for the five thermal bands: band 10 (8.1–8.5 μm), band 11 (8.5–8.9 μm), band 12 (8.9–9.3 μm), band 13 (10.3–11.0 μm) and band 14 (11.0–11.70 μm) (Fig. 2). The mathematical equation to be used for convolution bandpass is presented as follows (1):

$$\varepsilon_f = \frac{\int \varepsilon_\lambda \delta_\lambda \mathrm{d}_\lambda}{\int \delta_\lambda \mathrm{d}_\lambda}, \tag{1}$$

where ε_f is the effective emissivity, ε_λ is the spectral emissivity, and δ_λ is the system response function. Except for the spodosol class, the ASL soils show a high dispersion in the first three ASTER thermal bands (between 8 and 9.5 μm), whereas this dispersion is minimized in a classical split-window region between 10 and 12 μm. A similar comparison was also presented in [14]. All samples present a slight decreasing of emissivity value near 9 μm before an abrupt increase. In the spodosol class, the emissivity

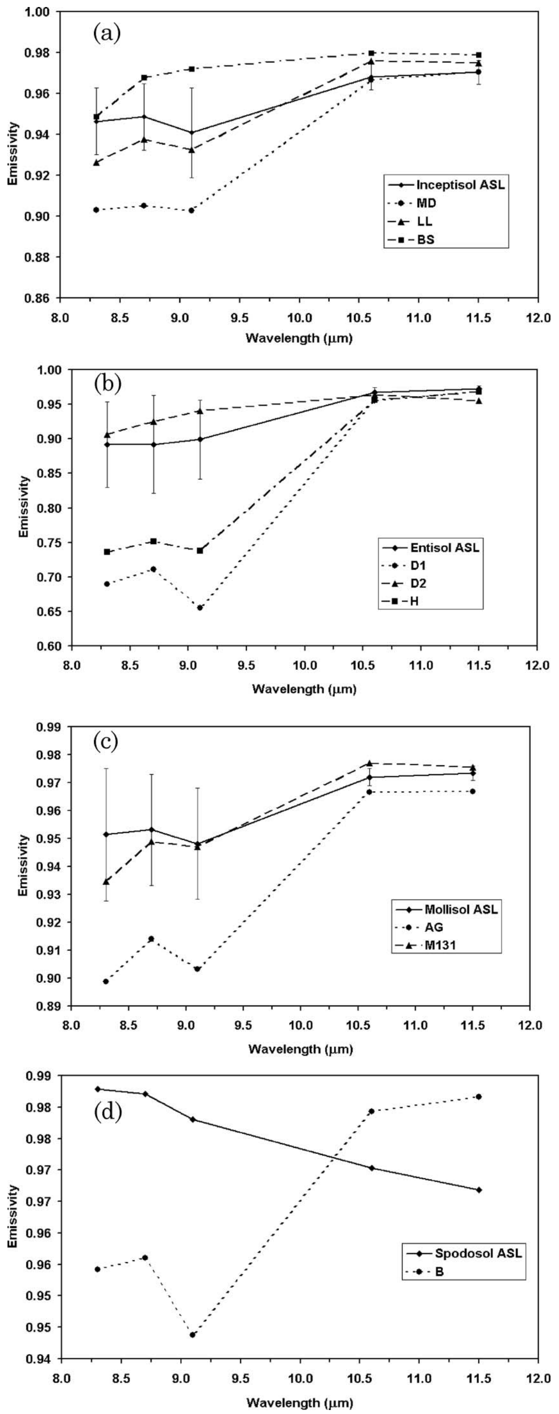

Fig. 2. Emissivity mean values of MD, LL, BS, and the seven spectra related with inceptisol orders provided by the JPL for each ASTER thermal bands. (a) Inceptisol refers to the mean value for seven samples, (b) entisol and (c) mollisol for 10 and nine samples, respectively, and (d) spodosol for only one.

spectra extracted from the ASL contain glass but there are no strong peaks in the emissivity spectra, which suggests the glass is amorphous rather than crystalline. The B soil spectrum shows mineralogical peaks, attributed to quartz (near 12 μm). In addition, XRD analysis shows a high content of this mineral, which could explain the different results between ASL and B spodosol class.

D. Comparison with Ground-Based Measurements

Surface emissivities can be retrieved from ground-based measurements collected with multiband radiometers by applying the temperature and emissivity separation (TES) algorithm, which utilizes a "calibration curve" to recover the surface emissivity [13,14]. This algorithm has also been applied to ground-based measurements [15,16]. Therefore, we have applied the algorithm to the band-averaged data and compared the emissivity retrieved with the actual emissivity measured in the laboratory.

Ground-based measurements were collected with a CIMEL CE 312-2 radiometer, with five thermal narrow bands similar to the ASTER ones, plus one broadband (8–14 μm). Details of the technical characteristics of the instrument can be found in [15,16]. A diffuse reflectance standard plate (Infragold from Labsphere Inc.) was also used to measure the sky downwelling irradiance. Except for sample BS, which was measured *in situ* during the corresponding field campaign, the rest of samples were measured outdoors during January 2008 at the University of Valencia, Spain. Measurements were carried out under clear-sky conditions and calm winds. Soil samples were placed on the ground, covering a spot of 30× 30 × 3 cm.. Twelve measurements were made of each sample. Samples CH and P were not measured, since there was insufficient material to cover the radiometer field of view. For the comparison, spectra retrieved from FT-IR spectroscopy were averaged to the CIMEL bands using its spectral response functions.

Results are presented in Table 3, and show good agreement between the ground-based measurements and laboratory measurements, with a total bias of 0.011 and a standard deviation (1-sigma) of 0.009. The total root mean square error (RMSE) was below 0.015, which is the nominal accuracy of the TES algorithm [13]. These small differences are attributed to slight differences in the sample preparation and application of the TES algorithm to the CIMEL data to obtain the emissivity.

E. Band-Averaged Emissivities for Common Thermal Remote Sensing Sensors

Finally, we provide band-averaged emissivity values (using sensor bands spectral response functions) for common thermal remote sensing sensors, such as ASTER onboard the Terra platform, Thematic Mapper (TM) onboard the Landsat-5 platform, Advanced Very High Resolution Radiometer (AVHRR) onboard the National Oceanic and Atmospheric Administration (NOAA)-18 platform and Moderate Resolution Imaging Spectroradiometer (MODIS) on board the Terra and Aqua platforms. The results are presented in Table 4. These band emissivity values can be considered as a reference to apply methods for land surface temperature retrieval (as, for example, single channel or split window) in which the knowledge of surface emissivity is required.

Table 3. Emissivity Values Retrieved by Filtered Spectrum and the TES Algorithm[a]

	8.1–8.5	8.5–8.9	8.9–9.3	10.3–11.0	11.3–11.7	Bias	σ	RMSE
AG	0.009	0.007	0.008	0.006	0.006	0.007	0.001	0.007
B	0.017	0.030	0.022	0.014	0.018	0.020	0.006	0.021
BS	0.000	0.000	0.000	0.000	0.000	0.000	0.000	0.000
D1	0.003	0.028	0.011	0.012	0.014	0.013	0.009	0.016
D2	−0.009	−0.007	−0.007	−0.002	−0.005	−0.006	0.002	0.006
H	0.003	0.020	0.016	0.013	0.014	0.013	0.006	0.015
M131	0.015	0.016	0.017	0.011	0.011	0.014	0.003	0.014
LL	0.018	0.016	0.015	0.011	0.012	0.014	0.003	0.014
MD	0.022	0.022	0.025	0.012	0.012	0.018	0.006	0.019
					TOTAL	0.011	0.009	0.014

[a]Also shown were the bias, σ, and RMSE between each sample and the total.

Table 4. Emissivity Filtered Values of Soil Spectra Applied to Different Common Thermal Sensors

	Banwidth (μm)	Effective Wavelength (μm)	AG	B	BS	CH	D1	D2	H	LL	M131	MD	P
ASTER	8.1–8.5	8.3	0.899	0.954	0.949	0.981	0.689	0.906	0.736	0.926	0.935	0.903	0.962
	8.5–8.9	8.7	0.914	0.956	0.968	0.970	0.711	0.925	0.752	0.938	0.949	0.905	0.963
	8.9–9.3	9.1	0.903	0.944	0.972	0.959	0.655	0.941	0.737	0.932	0.947	0.903	0.957
	10.3–11.0	10.6	0.967	0.979	0.980	0.966	0.955	0.964	0.956	0.976	0.977	0.966	0.980
	11.3–11.7	11.5	0.967	0.982	0.979	0.970	0.968	0.955	0.968	0.975	0.976	0.971	0.978
Landsat-4	10.3–12.4	11.1	0.968	0.980	0.982	0.970	0.965	0.960	0.966	0.976	0.977	0.970	0.979
Landsat-5	10.5–12.4	11.4	0.971	0.984	0.981	0.972	0.970	0.960	0.970	0.978	0.979	0.973	0.980
Landsat-7	10.3–12.4	10.5	0.970	0.980	0.983	0.971	0.966	0.961	0.967	0.977	0.978	0.971	0.980
NOAA-18	10.3–11.3	10.8	0.967	0.980	0.980	0.967	0.958	0.961	0.959	0.976	0.977	0.967	0.979
	11.5–12.5	12.0	0.976	0.989	0.983	0.977	0.976	0.962	0.978	0.982	0.981	0.978	0.983
MODIS	2.1–2.2	2.1	0.573	0.647	0.601	0.786	0.508	0.401	0.488	0.705	0.705	0.504	0.962
Terra	3.7–3.8	3.8	0.793	0.902	0.825	0.793	0.714	0.834	0.731	0.827	0.805	0.800	0.969
	4.0–4.1	4.1	0.769	0.891	0.824	0.786	0.725	0.864	0.729	0.816	0.793	0.815	0.970
	4.4–4.5	4.5	0.818	0.917	0.850	0.826	0.906	0.806	0.866	0.852	0.833	0.917	0.972
	6.5–6.9	6.8	0.985	0.990	0.936	0.990	0.997	0.951	0.996	0.984	0.972	0.985	0.982
	7.2–7.5	7.3	0.985	0.991	0.942	0.987	0.997	0.953	0.996	0.983	0.972	0.986	0.982
	10.8–11.3	11.0	0.967	0.980	0.981	0.969	0.963	0.960	0.964	0.976	0.977	0.969	0.979
	11.8–12.3	12.0	0.978	0.990	0.984	0.977	0.984	0.962	0.983	0.983	0.982	0.979	0.983

4. Conclusions

In this study we have provided the emissivity spectra for a variety of soils, which can be used to evaluate land surface temperature algorithms for a variety of satellite sensors. The emissivity spectra presented were compared to other soil spectra included in the ASL and to surface emissivities retrieved from ground-based measurements. Results indicated a good agreement, with a RMSE bellow 0.015 and a high linear correlation coefficient ($R^2 = 0.988$). Future work will focus on the effect of particle size on the emissivity spectra of soils.

The authors thank J. Bastida and Mar Urquiola of the Industrial Mineral Laboratory at Department of Geology of the University of Valencia for their help in mineralogical soil analysis. The authors also thank, for supporting this paper in part, the Ministerio de Ciencia y Tecnología (TERMASAT, project ESP2005-07724-C05-04; EODIS, project AYA2008-0595-C04-01) and the European Union (CEOP-AEGIS, project FP7-ENV-2007-1 proposal 212921; WATCH, project 036946).

References

1. F. Becker, W. Ngai, and M. P. Stoll, "An active method for measuring thermal infrared effective emissivities: implications and perspectives for remote sensing," Adv. Space Res. **1**, 193–210 (1981).
2. J. A. Sobrino and J. Cuenca, "Angular variation of thermal infrared emissivity for some natural surfaces from experimental measurements," Appl. Opt. **38**, 3931–3936 (1999).
3. J. Cuenca and J. A. Sobrino, "Experimental measurements for studying angular and spectral variation of thermal infrared emissivity," Appl. Opt. **43**, 4598–4602 (2004).
4. J. W. Salisbury, A. Wald, and D. M. D'Aria, "Thermal-infrared remote sensing and Kirchhoffs's law. 1. Laboratory measurements," J. Geophys. Res. **99**, 11897–11911 (1994).
5. J. W. Salisbury, L. S. Walter, N. Vergo, and D. M. D'Aria, *Infrared (*2.1–25 μm*) Spectra of Minerals* (Johns Hopkins U. Press, 1991), p. 267.
6. P. Christensen and S. T. Harrison, "Thermal infrared emission spectroscopy of natural surfaces: application to desert varnish coatings and rocks," J. Geophys. Res. **98**, 19819–19834 (1993).
7. P. R. Christensen, J. L. Bandfield, V. E. Hamilton, D. A. Howard, M. E. Lane, J. L. Piatek, S. W. Ruff, and W. L. Stefanov, "A thermal emission spectral library of rock forming minerals," J. Geophys. Res. **105**, 9735–9738 (2000).
8. http://speclib.asu.edu/.

9. A. M. Baldridge, S. J. Hook, C. I. Grove, and G. Rivera, "The ASTER spectral library version 2.0," Remote Sens. Environ. **113**, 711–715 (2009).
10. http://speclib.jpl.nasa.gov/.
11. F. E. Nicodemus, "Directional reflectance and emissivity of an opaque surface," Appl. Opt. **4**, 767–773 (1965).
12. S. J. Hook, J. E. Dmochowski, K. A. Howard, L. C. Rowan, K. E. Karlstrom, and J. M. Stock, "Mapping variations in weight percent silica measured from multispectral thermal infrared imagery—Examples from the Hiller Mountains, Nevada, USA and Tres Virgenes-La Reforma, Baja California Sur, Mexico," Remote Sens. Environ. **95**, 273–289 (2005).
13. A. Gillespie, S. Rokugawa, T. Matsunaga, J. S. Cothern, S. J. Hook, and A. B. Kahle, "A temperature and emissivity separation algorithm for advance spaceborne thermal emission and reflection radiometer (ASTER) images," IEEE Trans. Geosci. Remote Sens. **36**, 1113–1126 (1998).
14. P. S. Kealy and S. J. Hook, "Separating temperature and emissivity in thermal infrared multispectral scanner data: implications for recovering land surface temperatures," IEEE Trans. Geosci. Remote Sens. **31**, 1155–1164 (1993).
15. V. Payan and A. Royer, "Analysis of temperature and emissivity separation (TES) algorithm applicability and sensitivity," Int. J. Remote Sens. **25**, 15–37 (2004).
16. J. C. Jiménez-Muñoz and J. A. Sobrino, "Emissivity spectra obtained from field and laboratory measurements using the temperature and emissivity separation algorithm," Appl. Opt. **45**, 7104–7109 (2006).